IEEE Access
Multidisciplinary | Rapid Review | Open Access Journal

Received February 21, 2020, accepted March 16, 2020, date of publication March 20, 2020, date of current version April 1, 2020.

Digital Object Identifier 10.1109/ACCESS.2020.2982185

Kinematic Design of a 2R1T Robotic End-Effector With Flexure Joints

GUILIN YANG[1,3], (Member, IEEE), RENFENG ZHU[1,2], ZAOJUN FANG[1,3], CHIN-YIN CHEN[1,3], (Member, IEEE), AND CHI ZHANG[1,3], (Senior Member, IEEE)

[1]Ningbo Institute of Materials Technology and Engineering, Chinese Academy of Sciences, Ningbo 315201, China
[2]College of Materials Sciences and Opto-Electronic Technology, University of Chinese Academy of Sciences, Beijing 100049, China
[3]Zhejiang Key Laboratory of Robotics and Intelligent Manufacturing Equipment Technology and Engineering, Ningbo 315201, China

Corresponding authors: Guilin Yang (glyang@nimte.ac.cn) and Zaojun Fang (fangzaojun@nimte.ac.cn)

This work was supported in part by the National Key Research and Development Program of China under Grant 2018YFB1308900, in part by the NSFC-Zhejiang Joint Found for the Integration of Industrialization and Informatization under Grant U1509202, in part by the NSFC-Shenzhen Robotic Fundamental Research Center Project under Grant U1813223, in part by The Scientific Innovation Team Project of Ningbo—the Innovation Team of Key Components and Technology for the New Generation Robot under Grant 2016B10016, and in part by the Ningbo International Cooperation Project under Grant 2017D10023.

ABSTRACT This paper focuses on the kinematic design issues for a three *degrees-of-freedom* (DOFs), i.e., *two-rotational and one-translational* (2R1T) end-effector to perform continuous contact operations, such as deburring, grinding, and polishing. The proposed end-effector design employs a 3-legged *prismatic-prismatic-spherical* (3-PPS) parallel mechanism due to its desired kinematic characteristics and dynamic behavior. As the 3-PPS parallel mechanism is featured with zero-torsion motion characteristic, the orientation of its moving platform can be always represented by a rotation about an axis parallel to its base platform plane. Through analysis of the rotation matrix of the moving platform, closed-form linear solutions for both forward and inverse displacement analyses are readily derived. Other critical design issues, such as passive prismatic joint displacement, parasitic motion, velocity, and singularity analyses, are addressed. For a specific dimension design of the 3-PPS parallel mechanism, the workspace analysis indicates that the proposed design can achieve a singularity-free $\pm 12^\circ \times \pm 12^\circ \times 25$ mm workspace. Furthermore, as the displacements of the passive prismatic joints are within 2.63 mm, light-weight flexure-based prismatic joints are designed to replace the conventional heavy linear guides. The flexure-rigid structure of the 3-DOF 2R1T end-effector significantly improves the dynamic performance of the system. A prototype of the 3-DOF 2R1T robotic end-effector is designed and fabricated to verify the proposed design.

INDEX TERMS Kinematic design, 3-DOF 2R1T parallel mechanism, robotic end-effector, flexure joints.

I. INTRODUCTION

Surface finishing, e.g., grinding and polishing, is a key process for workpiece quality enhancement in precision engineering. However, many surface finishing tasks are still performed manually by skilled workers, which leads to low efficiency, inconsistence in finishing quality, and hazardous work environment [1]–[3]. To address the problems of manual surface finishing, robotic finishing is a promising solution, which has drawn extensive attention from both academia and industry for not only cost effectiveness but also quality consistence [4]–[6].

The associate editor coordinating the review of this manuscript and approving it for publication was Rui-Jun Yan.

As surface finishing involves continuous contact operations, force control is crucial for robotic finishing [7]. There are mainly two approaches, i.e., ''around-the-arm'' approach and ''through-the-arm'' approach, to achieve active force control [1], [8]. As industrial robots employed for surface finishing applications usually have large moving mass and closed control architecture, it is difficult for the ''through-the-arm'' approach to achieve precise force control. In comparison, the ''around-the-arm'' approach based on an add-on force-controlled end-effector is a more suitable option for industrial robots to achieve active force control [1], [8], [9].

An industrial robot with a force-controlled end-effector is a macro-mini manipulator system. During continuous contact operations, the industrial robot, i.e., the macro manipulator,

will only perform motion control to track the desired trajectories, while the force-controlled end-effector, i.e., the mini manipulator, will regulate the contact force. With effective coordination strategies, such a macro-mini manipulator system posses the advantages of large workspace provided by the macro manipulator and high dynamic response provided by the mini manipulator [10]–[12]. Therefore, an industrial robot with an add-on force-controlled end-effector is able to achieve high force control bandwidth and accuracy for precision surface finishing applications.

As the industrial robots are well developed and commercial available, the development of high-performance force-controlled end-effectors becomes a major research issue. Most of the commercial available force-controlled end-effectors employ 1-DOF design and are driven by pneumatic actuators, which suffer from low dexterity and slow dynamic response. As for curved surface finishing, an industrial robot equipped with a 3-DOF 2R1T force-controlled end-effector is an ideal solution. To achieve 3-DOF 2R1T motions, end-effectors based on the parallel mechanisms have drawn particular attention due to their inherent advantages such as low moving mass, high stiffness, large loading capability, and high positioning accuracy [13]–[15]. Among various 3-DOF 2R1T parallel mechanisms, a class of 3-[XX]S (''X'' stands for either a Prismatic joint or a Revolute joint, and ''S'' stands for a Spherical joint) parallel mechanisms with zero-torsion motion characteristic are suitable candidates due to their symmetric configurations, simple kinematics, and compact structure designs. A successful application of the 3[XX]S parallel mechanism is the Sprint Z3 tool head developed by DS Technologies, which employed a 3-PRS configuration [16], [17]. However, the heavy duty Sprint Z3 tool head is large in size and lacks force control capabilities, which is not applicable for force-controlled robotic end-effectors.

The kinematic design issues of the 3-[XX]S parallel mechanisms have been investigated by a number of researchers [18]–[22]. In [18], Li et.al. investigated a 3-PRS parallel manipulator with adjustable layout angle of actuators for different tasks. In [19], Liu et.al. investigated kinematic and dynamic issues of a 3-RRS parallel mechanism. In [20], Bonev proposed a modified Euler angles method and derived the closed-form direct kinematic solutions for three kinds of zero-torsion parallel mechanisms, i.e. 3-PPS, 3-PRS, and 3-RPS parallel mechanisms. In [21], Huang et.al. studied the instantaneous motions of the 3-RPS parallel mechanisms by the kinematic influence coefficient matrices. In [22], Schadlbauer et.al. analyzed two different operation modes of 3-RPS parallel mechanisms based on an algebraic approach. However, the unique characteristics of the rotation matrix of the 3-[XX]S parallel mechanism with zero-torsion motion are not well studied and utilized for kinematics analysis.

This paper focuses on the kinematic design issues of a 3-DOF 2R1T end-effector for robotic finishing applications. A symmetric 3-PPS parallel mechanism is employed in this work owing to its advantages of simple kinematics, large singularity-free workspace, compact and light-weight structure, and desired motion and force control performance. Due to the mechanism's zero-torsion motion characteristic, the orientation of its moving platform can be always represented by a rotation about an axis parallel to its base platform plane. Consequently, the rotation matrix of the moving platform possesses some unique features. In light of the geometric representation of moving platform orientation, interesting relationships about the entries of the rotation matrix have been identified. Based on such relationships as well as the perpendicular arrangement of the two prismatic joints in each leg, closed-form linear solutions for both forward and inverse displacement analyses are readily derived. Furthermore, the moving platform workspace analysis of a specific end-effector design indicates that the passive prismatic joint displacements are within 2.63 mm. Therefore, light-weight flexure-based prismatic joints are designed to replace the conventional heavy linear guides, which can significantly reduce the moving mass and improve the dynamic performance of the 2R1T end-effector.

The rest of this paper is organized as follows. In Section II, the rationales for choosing the 3-PPS parallel mechanisms are elaborated. In Section III, closed-form linear solutions for both forward and inverse displacement analyses are derived based on a thorough analysis of the rotation matrix of the moving platform. The passive prismatic joint displacement, parasitic motion, velocity, and singularity analyses are also addressed. In Section IV, workspace analysis is presented based on a finite partition scheme. In Section V, the stiffness and deflection of the flexure-based passive joints are analyzed, and a prototype of the 3-DOF 2R1T end-effector is developed. Finally, Section VI summarizes the paper.

II. CONFIGURATION DESIGN

In order to fulfill the requirements of curved surface finishing process, the class of 3-[XX]S parallel mechanisms with zero-torsion motion characteristic are considered as the suitable candidates for the 3-DOF 2R1T end-effector design. The possible parallel mechanism configurations whose moving platform is supported by three identical legs are investigated. Three types of joints, including 1-DOF R-joint, 1-DOF P-joint, and 3-DOF-S joint, are considered.

The feasible 3-[XX]S configurations are enumerated, i.e., 3-RRS, 3-RPS, 3-PRS, and 3-PPS. Among them, the 3-PPS configuration has simple kinematics, large singularity-free workspace, and high accuracy. In addition, the 3-PPS configuration has identical actuation directions such that it has the same performance along its actuation directions [23]. Therefore, the 3-PPS configuration is a promising candidate for the 3-DOF 2R1T end-effector design.

As shown in Fig. 1, the proposed 3-PPS configuration consists of a base platform, three identical PPS legs and a moving platform. The three identical legs are placed 120° apart in order to have a symmetric design. The first prismatic joint in each leg is selected as the active joint, and it is

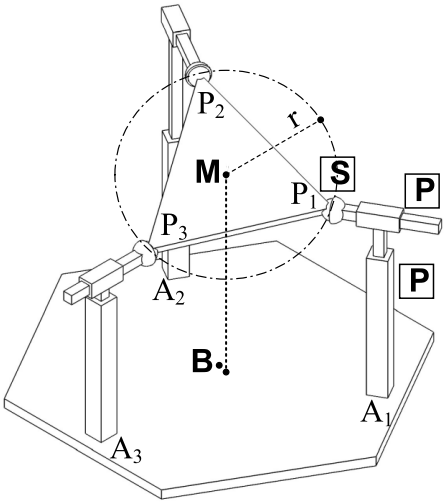

FIGURE 1. Schematic of a 3-PPS parallel mechanism.

directly attached to the base platform to reduce the moving mass. The second prismatic joint in each leg is selected as a passive joint. Furthermore, the three active prismatic joints are placed vertically, while the three passive prismatic joints are placed horizontally with their translational directions pointing to the center of the base platform. The passive spherical joint in each leg is directly attached to the moving platform.

III. KINEMATIC ANALYSIS

In this section, based on the zero-torsion motion characteristic of the 3-PPS parallel mechanism, the rotation matrix of the moving platform is investigated through symbolic computation. Some unique relationships about the entries of the rotation matrix have been identified in light of the geometric representation of moving platform orientation. Forward and inverse displacement analyses are significantly simplified and closed-form solutions are readily derived through a simple comparison between two different parametric forms of the rotation matrices. The passive prismatic joint displacement and the parasitic motion of the moving platform are analyzed. The velocity and singularity analyses are also addressed.

As shown in Fig. 2, both the base frame $\{B\}$ and the moving platform frame $\{M\}$ are right-hand Cartesian coordinate frames. An equilateral triangular base plate is defined by three PPS chain's attachment points, i.e., A_1, A_2, and A_3. The base frame $\{B\}$ is fixed at the center of the base plate with its Z-axis perpendicular to the base plate and X-axis parallel to A_2A_3. Similarly, the equilateral triangular moving platform is defined by the centers of the three spherical joints, i.e., P_1, P_2, and P_3. The moving platform frame $\{M\}$ is attached to the center of the equilateral triangular moving platform with its z-axis perpendicular to the moving platform and x-axis parallel to P_2P_3. Define r as the circumcircle radius of the equilateral triangular moving platform. The local coordinates of points $P_i(i = 1, 2, 3)$ with respect to the moving platform

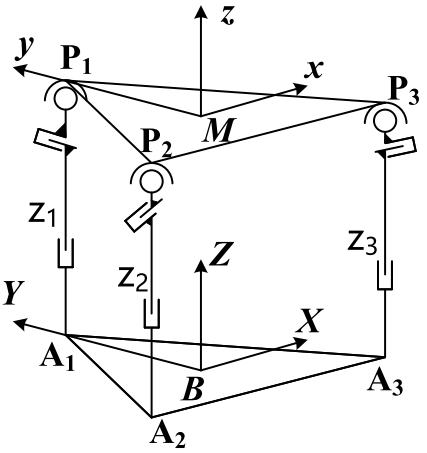

FIGURE 2. Kinematic diagram of a 3-PPS parallel mechanism.

frame $\{M\}$, denoted by $P_{iM}(i = 1, 2, 3)$, are:

$$\begin{cases} P_{1M} = (0, r, 0) \\ P_{2M} = \left(-\dfrac{\sqrt{3}r}{2}, -\dfrac{r}{2}, 0\right) \\ P_{3M} = \left(\dfrac{\sqrt{3}r}{2}, -\dfrac{r}{2}, 0\right) \end{cases} \tag{1}$$

As the active prismatic joint in each leg is placed vertically and the passive prismatic joint is placed horizontally, the global coordinates of $P_i(i = 1, 2, 3)$ with respect to the base frame $\{B\}$, denoted by $P_{iB}(i = 1, 2, 3)$, are given by:

$$\begin{cases} P_{1B} = (0, y_1, z_1) \\ P_{2B} = \left(\sqrt{3}y_2, y_2, z_2\right) \\ P_{3B} = \left(-\sqrt{3}y_3, y_3, z_3\right) \end{cases} \tag{2}$$

A. FORWARD DISPLACEMENT ANALYSIS

As shown in Fig. 2, define $\boldsymbol{T}_{BM} \in SE(3)$ to describe the moving platform frame $\{M\}$ relative to the base frame $\{B\}$, then we get:

$$\begin{bmatrix} P_{1B} & P_{2B} & P_{3B} \\ 1 & 1 & 1 \end{bmatrix} = \boldsymbol{T}_{BM} \begin{bmatrix} P_{1M} & P_{2M} & P_{3M} \\ 1 & 1 & 1 \end{bmatrix} \tag{3}$$

Since both frames $\{B\}$ and $\{M\}$ are right-hand Cartesian coordinate frames, we also have

$$\begin{pmatrix} \boldsymbol{P}_{12B} \times \boldsymbol{P}_{23B} \\ 0 \end{pmatrix} = \boldsymbol{T}_{BM} \begin{pmatrix} \boldsymbol{P}_{12M} \times \boldsymbol{P}_{23M} \\ 0 \end{pmatrix} \tag{4}$$

where $\boldsymbol{P}_{12B} = P_{2B} - P_{1B}$, $\boldsymbol{P}_{23B} = P_{3B} - P_{2B}$, $\boldsymbol{P}_{12M} = P_{2M} - P_{1M}$, and $\boldsymbol{P}_{23M} = P_{3M} - P_{2M}$.

Combining (3) and (4), it is straightforward to derive that

$$\boldsymbol{T}_{BM} = \begin{bmatrix} \boldsymbol{R}_{BM} & \boldsymbol{M}_{BM} \\ \boldsymbol{0}_{1\times 3} & 1 \end{bmatrix} \tag{5}$$

where $\boldsymbol{R}_{BM} \in SO(3)$ and $\boldsymbol{M}_{BM} \in \mathbb{R}^{3\times 1}$ are given as follows:

$$\boldsymbol{R}_{BM} = \begin{bmatrix} -\dfrac{y_2+y_3}{r} & \dfrac{y_3-y_2}{\sqrt{3}r} \\ \dfrac{y_3-y_2}{\sqrt{3}r} & -\dfrac{-2y_1+y_2+y_3}{3r} \\ \dfrac{z_3-z_2}{\sqrt{3}r} & -\dfrac{-2z_1+z_2+z_3}{3r} \end{bmatrix} \begin{matrix} \dfrac{2\left(y_3\left(z_1-z_2\right)+y_1\left(z_2-z_3\right)+y_2\left(z_3-z_1\right)\right)}{3\sqrt{3}r^2} \\ \dfrac{2\left(y_3\left(z_1-z_2\right)+y_2\left(z_1-z_3\right)\right)}{3r^2} \\ \dfrac{4y_2y_3-2y_1\left(y_2+y_3\right)}{3r^2} \end{matrix} \tag{6}$$

$$\boldsymbol{M}_{BM} = \left(\frac{y_2-y_3}{\sqrt{3}} \quad \frac{y_1+y_2+y_3}{3} \quad \frac{z_1+z_2+z_3}{3}\right)^T \tag{7}$$

As the expressions of $\boldsymbol{R}_{BM}$ and $\boldsymbol{M}_{BM}$ contain variables other than the active joint displacement $z_i (i = 1, 2, 3)$, the expression of $\boldsymbol{T}_{BM}$ needs to be further evaluated.

According to the rotation matrix formulated in (6), it is observed that the entry of the first row and the second column is equal to the entry of the second row and the first column, i.e., $\boldsymbol{R}_{BM}(1, 2) = \boldsymbol{R}_{BM}(2, 1)$, which also implies the unique zero-torsion motion characteristic.

Recall that any orientation matrix $\boldsymbol{R} \in SO(3)$ can be always realized by a rotation about a unit vector $\boldsymbol{\omega} = (\omega_x, \omega_y, \omega_z) \in \mathbb{R}^{3\times 1}$ with an angle $\theta \in [0, 2\pi)$. According to the Rodrigues' formula, such a rotation, represented by $e^{\hat{\boldsymbol{\omega}}\theta} \in SO(3)$, can be computed by

$$e^{\hat{\boldsymbol{\omega}}\theta} = \boldsymbol{I}_{3\times 3} + \hat{\boldsymbol{\omega}} \sin\theta + \hat{\boldsymbol{\omega}}^2 (1 - \cos\theta) \tag{8}$$

where $\hat{\boldsymbol{\omega}} \in so(3)$ is the skew symmetric matrix associated with $\boldsymbol{\omega} \in \mathbb{R}^{3\times 1}$.

In (6), as $\boldsymbol{R}_{BM}(1, 2) = \boldsymbol{R}_{BM}(2, 1)$ and it yields $\omega_z = 0$. Equation (8) can be simplified as:

$$\boldsymbol{R}_{BM} = \begin{bmatrix} \cos\theta + \omega_x^2 v_\theta & \omega_x\omega_y v_\theta & \omega_y \sin\theta \\ \omega_x\omega_y v_\theta & \cos\theta + \omega_y^2 v_\theta & -\omega_x \sin\theta \\ -\omega_y \sin\theta & \omega_x \sin\theta & \cos\theta \end{bmatrix} \tag{9}$$

where $v_\theta = (1 - \cos\theta)$.

Equation (9) also indicates that $\boldsymbol{R}_{BM}(1, 3) = -\boldsymbol{R}_{BM}(3, 1)$, $\boldsymbol{R}_{BM}(2, 3) = -\boldsymbol{R}_{BM}(3, 2)$ and $\boldsymbol{R}_{BM}(1, 1) + \boldsymbol{R}_{BM}(2, 2) - \boldsymbol{R}_{BM}(3, 3) = 1$. The aforementioned analysis leads to a conclusion that the rotation motion of the 3-PPS moving platform can be always represented by a rotation about an axis which is parallel to the base platform plane [24]. Such interesting relationships derived from the zero-torsion motion characteristic can be utilized to derive the equivalent expressions of the rotation matrix and significantly simplify the following displacement analysis.

Based on the zero-torsion motion characteristic of the 3-PPS parallel mechanism, the rotation axis, i.e., the unit directional vector $\boldsymbol{\omega}$, and the tilting angle θ can be readily determined. As shown in Fig. 3, the moving platform frame coincides with the reference frame XYZ initially. If we rotate

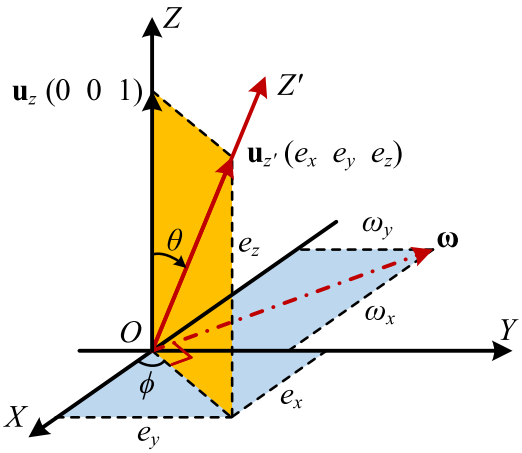

FIGURE 3. Rotation about an unit axis ω parallel to base plane.

the moving platform frame about the unit directional vector $\boldsymbol{\omega}$ in the reference frame's XY plane with an angle θ, the Z'-axis of the moving platform frame, i.e., OZ', can be obtained. Assume that the unit directional vector of the Z'-axis is given by $\boldsymbol{u}_{z'} = (e_x, e_y, e_z)$, such that $e_x^2 + e_y^2 + e_z^2 = 1$, we have:

$$\begin{cases} \sin\theta = \sqrt{e_x^2 + e_y^2} \\ \cos\theta = \sqrt{1 - e_x^2 - e_y^2} \end{cases} \tag{10}$$

In (10), if we limit the tilting angle $\theta \in [0, \pi/2]$, both $\sin\theta$ and $\cos\theta$ can be uniquely determined.

As the unit directional vector of the Z-axis of the reference frame is given by $\boldsymbol{u}_z = (0, 0, 1)$, the unit directional vector $\boldsymbol{\omega}$ is the cross product of $\boldsymbol{u}_z$ and $\boldsymbol{u}_{z'}$, which is determined by:

$$\boldsymbol{\omega} = \frac{\boldsymbol{u}_z \times \boldsymbol{u}_{z'}}{\left\|\boldsymbol{u}_z \times \boldsymbol{u}_{z'}\right\|} = \left(-\frac{e_y}{\sqrt{e_x^2+e_y^2}} \quad \frac{e_x}{\sqrt{e_x^2+e_y^2}} \quad 0\right)^T \tag{11}$$

Substituting (10) and (11) into (9), we derive the equivalent expression of the rotation matrix which is given by:

$$\boldsymbol{R}_{BM} = \begin{bmatrix} \dfrac{e_x^2 e_z + e_y^2}{e_x^2+e_y^2} & \dfrac{e_x e_y (e_z - 1)}{e_x^2+e_y^2} & e_x \\ \dfrac{e_x e_y (e_z - 1)}{e_x^2+e_y^2} & \dfrac{e_x^2 + e_y^2 e_z}{e_x^2+e_y^2} & e_y \\ -e_x & -e_y & e_z \end{bmatrix} \tag{12}$$

where $e_z = \sqrt{1 - e_x^2 - e_y^2}$ when $\theta \in [0, \pi/2]$.

By comparing (6), (7) and (12), we can readily obtain the closed-form solutions for the forward displacement of the 3-PPS configuration, which have simple linear forms as:

$$\begin{cases} e_x = \dfrac{z_2 - z_3}{\sqrt{3}r} \\ e_y = \dfrac{-2z_1 + z_2 + z_3}{3r} \\ m_z = \dfrac{z_1 + z_2 + z_3}{3} \end{cases} \tag{13}$$

where m_z represents the z-coordinate (i.e., the vertical displacement) of the moving platform frame $\{M\}$ with respect

to the base frame $\{B\}$. According to the above closed-form forward displacement solutions, when the three independent active prismatic joint displacements, i.e., z_1, z_2, and z_3, are given, the pose of moving platform can be readily determined. Furthermore, the solution is unique as long as the tilting angle $\theta \in [0, \pi/2]$.

B. INVERSE DISPLACEMENT ANALYSIS

According to the linear form of (13), the inverse displacement solutions for the 3-PPS configuration can be readily derived as follows:

$$\begin{cases} z_1 = m_z - re_y \\ z_2 = \dfrac{1}{2}\left(\sqrt{3}re_x + re_y + 2m_z\right) \\ z_3 = \dfrac{1}{2}\left(-\sqrt{3}re_x + re_y + 2m_z\right) \end{cases} \tag{14}$$

Notice that the inverse displacement solutions are also linear functions of three independent kinematics parameters of the moving platform. According to the above closed-form inverse displacement solutions, when the three independent kinematics parameters of the moving platform, i.e., e_x, e_y, and m_z, are given, the three active prismatic joint displacements can be readily determined. Furthermore, the solution is unique as long as the tilting angle $\theta \in [0, \pi/2]$.

C. PASSIVE PRISMATIC JOINT DISPLACEMENT ANALYSIS

According to the forward displacement analysis, each of the three passive prismatic joints displacements $d_i (i = 1, 2, 3)$, defined as the displacement from its home position (i.e., its position at $z_1{=}z_2{=}z_3{=}0$) to its current position along with its translational direction, can be readily determined as:

$$\begin{cases} d_1 = y_1 - r \\ d_2 = -2y_2 - r \\ d_3 = -2y_3 - r \end{cases} \tag{15}$$

In (15), $d_i (i = 1, 2, 3)$ is a function of $y_i (i = 1, 2, 3)$. According to (6) as well as the entries' relationships depicted from (12), $y_i (i = 1, 2, 3)$ can be determined with the active joint displacements $z_i (i{=}1, 2, 3)$, which are given as follows:

$$\begin{cases} y_1 = \dfrac{(z_1-z_2)(z_1-z_3)\,s - r(z_1+z_2-2z_3)(z_1-2z_2+z_3)}{2t} \\ y_2 = \dfrac{(z_1-z_2)(z_2-z_3)\,s - r(z_1+z_2-2z_3)(2z_1-z_2-z_3)}{4t} \\ y_3 = \dfrac{(z_1-z_3)(z_3-z_2)\,s - r(2z_1-z_2-z_3)(z_1-2z_2+z_3)}{4t} \end{cases} \tag{16}$$

where $s{=}\sqrt{9\,r^2 - 2\,(z_1-z_2)^2 - 2\,(z_1-z_3)^2 - 2\,(z_2-z_3)^2}$, $t = z_1^2 + z_2^2 + z_3^2 - z_1\,z_2 - z_1\,z_3 - z_2\,z_3$.

D. PARASITIC MOTION ANALYSIS

According to (7), the moving platform center of the proposed 3-PPS parallel mechanism has parasitic translational motion along the x and y axis of the base frame, denoted by m_x and m_y, respectively. Combining (7), (13) and (16), the parasitic translational motion of the moving platform center can be determined with the three active joint displacements as:

$$\begin{cases} m_x = \dfrac{\sqrt{3}\,(2z_1 - z_2 - z_3)\,(z_2 - z_3)(s - 3r)}{12t} \\ m_y = \dfrac{\left((z_1-z_2)^2 + (z_1-z_3)^2 - 2\,(z_2-z_3)^2\right)(s-3r)}{12t} \\ \delta = \sqrt{m_x^2 + m_y^2} = \dfrac{|s - 3r|}{6} \end{cases} \tag{17}$$

where δ is the projection distance from the home position of the moving platform (i.e., its position at $z_1{=}z_2{=}z_3{=}0$) to its current position onto the XY plane of the base frame.

Alternatively, the parasitic translational motion of the moving platform center can be described with the three independent kinematic parameters of the moving platform, such that:

$$\begin{cases} m_x = -\dfrac{e_x e_y \left(\sqrt{r^2\left(1 - e_x^2 - e_y^2\right)} - r\right)}{e_x^2 + e_y^2} \\ m_y = \dfrac{\left(e_y^2 - e_x^2\right)\left(\sqrt{r^2\left(1 - e_x^2 - e_y^2\right)} - r\right)}{2\left(e_x^2 + e_y^2\right)} \\ \delta = \sqrt{m_x^2 + m_y^2} = \dfrac{r}{2}(1 - \sqrt{1 - e_x^2 - e_y^2}) \end{cases} \tag{18}$$

In (18), the projection distance δ only depends on the orientation of the moving platform, i.e., e_x and e_y. According to (10), the projection distance δ can be rewritten as:

$$\delta = \frac{r}{2}(1 - \cos\theta) \tag{19}$$

The relationship between the tilting angle θ and the projection distance δ is plotted as shown in Fig. 4.

From Fig. 4, it is depicted that when the tilting angle θ increases from 0 to $\pi/2$, the projection distance δ increases from 0 to $r/2$.

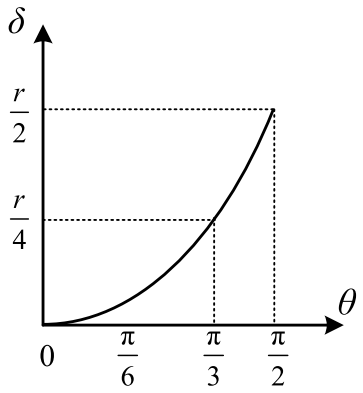

FIGURE 4. The projection distance δ as a function of the tilting angle θ.

E. VELOCITY ANALYSIS

Let vector $\overrightarrow{MP_i} (i = 1, 2, 3)$ be described in the base frame $\{B\}$ and its coordinates be $\left(MP_{ix}, MP_{iy}, MP_{iz}\right)$. The velocity of each spherical joint $\boldsymbol{V}_{PiB} (i = 1, 2, 3)$ can be obtained as

follows:

$$\boldsymbol{V}_{PiB} = \begin{pmatrix} \dot{x}_i \\ \dot{y}_i \\ \dot{z}_i \end{pmatrix} = -\overrightarrow{\boldsymbol{MP}_i} \times \boldsymbol{\Omega}_{BM} + \boldsymbol{V}_{BM} \tag{20}$$

where $\boldsymbol{V}_{BM} = (v_x, v_y, v_z)$ and $\boldsymbol{\Omega}_{BM} = (\varpi_x, \varpi_y, \varpi_z)$ are the linear velocity and the angular velocity of the moving platform with respect to the base frame $\{B\}$, respectively.

As the active prismatic joint in each leg is placed vertically and the passive prismatic joint in each leg is placed horizontally, the z component of each spherical joint velocity with respect to the base frame $\{B\}$ is equal to the velocity of the active prismatic joint in the same leg, such that:

$$\dot{z}_i = MP_{iy}\,\varpi_x - MP_{ix}\,\varpi_y + v_z \tag{21}$$

The velocity relationship between three active prismatic joints and moving platform can be readily obtained as:

$$\begin{pmatrix} \dot{z}_1 \\ \dot{z}_2 \\ \dot{z}_3 \end{pmatrix} = \begin{bmatrix} MP_{1y} & -MP_{1x} & 1 \\ MP_{2y} & -MP_{2x} & 1 \\ MP_{3y} & -MP_{3x} & 1 \end{bmatrix} \begin{pmatrix} \varpi_x \\ \varpi_y \\ v_z \end{pmatrix} \tag{22}$$

The entries (23) of the Jacobian matrix are shown at the bottom of this page.

F. SINGULARITY ANALYSIS

The parallel kinematic mechanism will gain or lose one or more DOFs at its singularities, thus singular configurations should be avoided in the design and applications.

Based on the velocity relationship between three active prismatic joints and the moving platform formulated in (22), the singularity analysis is conducted. The inverse, forward, and combined singularities can be identified based on rank analysis of the Jacobian matrix [25], [26]. As the inverse singularity normally occurs at the boundary of the workspace, it is not a very critical issue for parallel mechanisms. However, in a forward singularity, the mechanism will gain at least one DOF. As a forward singularity will make the mechanism uncontrollable, it is a very serious issue for parallel mechanism design. After symbolic computation, the determinant of Jacobian matrix is formulated as follows:

$$\det(\boldsymbol{J}) = \frac{3\sqrt{3}}{2} r^2 \sqrt{1 - e_x^2 - e_y^2} \tag{24}$$

In (24), $\det(\boldsymbol{J})$ will take the value of zero only if $e_x^2 + e_y^2 = 1$, i.e., $e_z = 0$ and $\theta = \pi/2$, which indicates that the equilateral triangular moving platform is perpendicular to the base plane. In such a case, the forward singularity will occur. The inverse singularity corresponds to a configuration where one leg reaches its motion limit, which can be readily avoided in our case. Thus the combined singularity where the inverse and forward singularities occur simultaneously can also be avoided. It can be further concluded that there does not exist any forward singularities within the entire workspace if $\theta \in [0, \pi/2)$.

IV. WORKSPACE ANALYSIS

Workspace is a critical performance index for parallel mechanism design. A numerical workspace analysis approach is presented in this section.

Considering the 3-DOF 2R1T motion of the 3-PPS parallel mechanism, the cylindrical coordinates, i.e., (θ, ϕ, m_z), are employed to represent the workspace of the moving platform, as shown in Fig. 5(a). In general, the ranges of the three cylindrical coordinates can be set as follows: $\theta \in [0, \pi/2)$, $\phi \in [-\pi, \pi)$, and $m_z \in [m_{z\min}, m_{z\max}]$, such that the maximum workspace of a 3-PPS parallel mechanism in cylindrical coordinates is a solid cylinder.

$$\begin{cases} MP_{1y} = \dfrac{r\left(e_y^2\sqrt{1-e_x^2-e_y^2}+e_x^2\right)}{e_x^2+e_y^2} \\ MP_{1x} = \dfrac{re_xe_y\left(\sqrt{1-e_x^2-e_y^2}-1\right)}{e_x^2+e_y^2} \\ MP_{2y} = -\dfrac{r\left[e_x^2+\sqrt{3}e_xe_y\left(\sqrt{1-e_x^2-e_y^2}-1\right)+e_y^2\sqrt{1-e_x^2-e_y^2}\right]}{2\left(e_x^2+e_y^2\right)} \\ MP_{2x} = -\dfrac{r\left[\sqrt{3}e_x^2\sqrt{1-e_x^2-e_y^2}+e_xe_y\left(\sqrt{1-e_x^2-e_y^2}-1\right)+\sqrt{3}e_y^2\right]}{2\left(e_x^2+e_y^2\right)} \\ MP_{3y} = -\dfrac{r\left[e_x^2-\sqrt{3}e_xe_y\left(\sqrt{1-e_x^2-e_y^2}-1\right)+e_y^2\sqrt{1-e_x^2-e_y^2}\right]}{2\left(e_x^2+e_y^2\right)} \\ MP_{3x} = \dfrac{r\left[\sqrt{3}e_x^2\sqrt{1-e_x^2-e_y^2}-e_xe_y\left(\sqrt{1-e_x^2-e_y^2}-1\right)+\sqrt{3}e_y^2\right]}{2\left(e_x^2+e_y^2\right)} \end{cases} \tag{23}$$

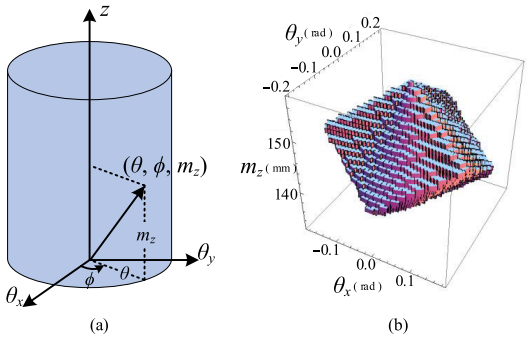

FIGURE 5. Workspace visualization: (a) cylindrical coordinates representation of the workspace; (b) isometric view of the workspace.

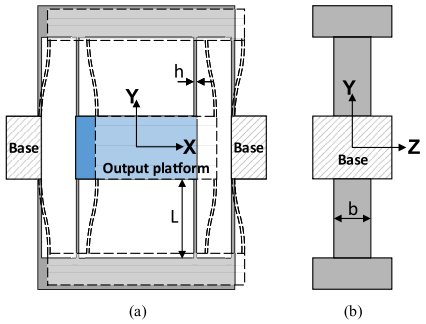

FIGURE 6. Double compound rectilinear flexure: (a) front view; (b) side view.

In this work, an equi-volumetric partition scheme of the parametric solid-cylinder workspace is employed, which can divide a solid cylinder into a number of elements with the same volume [27]. Utilizing a workspace elements detection algorithm based on the inverse displacement analysis formulated in (14), the resultant workplace with specific design parameters can be obtained. The *Mathematica* software tool is used for the implementation of workspace evaluation and visualization algorithms.

To design a 3-DOF 2R1T robotic end-effector for curved surface finishing applications, two major design requirements need to be satisfied, i.e., 12° for the tilting angle about the horizontal plane and 25 mm for the vertical translational displacement. The major kinematic design parameters to be determined are the circumcircle radius of the equilateral triangular moving platform and the stroke of the active prismatic joints. Note that the circumcircle radius of the equilateral triangular moving platform is the same as that of the equilateral triangular base platform. According to the inverse displacement analysis algorithm formulated in (14), we eventually take 25 mm for the strokes of the active prismatic joints and 80 mm for the circumcircle radius of the equilateral triangular moving platform r.

Based on the proposed kinematic design parameters, the resultant workplace is obtained. As shown in Fig. 5(b), the maximum values of tilting angle θ ($\theta = \sqrt{\theta_x^2 + \theta_y^2}$) and vertical translational range are 12° (i.e., 0.21 rad) and 25 mm, respectively. The initial length of the three active prismatic joints is equal to 132.5 mm and it varies between 132.5 mm to 157.5 mm. The results indicate that the kinematic design parameters can fulfill the workspace requirements for typical surface finishing applications.

V. PROTOTYPE DEVELOPMENT

Based on the kinematic design parameters proposed in this work, a prototype of the 3-PPS robotic end-effector is designed, which consists of a base platform, three identical PPS legs and a moving platform. Specifically, three identical legs are placed 120° apart. The first prismatic joint in each leg is selected as the active joint which is base-mounted and placed vertically. The second prismatic joint in each leg is selected as the passive prismatic joint which is placed horizontally. Three passive spherical joints(SRJ012C from HEPHAIST SEIKO), whose permissible swing angles are ±30°, are directly attached to the moving platform. To improve the dynamic response for active force control, three 25 mm-stroke *voice coil motors* (VCMs) are employed as the active prismatic joints. The circumcircle radius of the equilateral triangular moving platform r is equal to 80 mm. In this specific design, the displacement analysis of the passive prismatic joints indicates that the maximum displacement is within 2.63 mm according to (15) and (16).

Considering the small displacements of the three passive prismatic joints, a double compound rectilinear flexure mechanism is employed as the passive prismatic joint to replace the conventional heavy linear guides, which can significantly reduce the parasitic errors in off-axis directions, especially the parasitic errors in y-axis direction. In addition, to reduce the parasitic errors in z direction, the double compound rectilinear flexure mechanism is designed to achieve high stiffness ratio between z-axis and x-axis (the driving direction). The key geometric parameters of the double compound rectilinear flexure mechanism are shown in Fig. 6.

Based on the linear assumption and the boundary conditions of the deflection, the stiffness in the drive direction(x-axis) of the double compound rectilinear flexure is determined by [28]:

$$K_x = \frac{F_x}{x} = \frac{24EI}{L^3} = \frac{2Ebh^3}{L^3} \tag{25}$$

The transverse z-axis stiffness is determined by:

$$K_z = \frac{Ehb^3}{2L^3} \tag{26}$$

where L and h denote the length and width of the leaf flexure, respectively, while b denotes the thickness of the plate.

Consider that the maximum translation is constrained by the stress induced by the maximum force $F_{x\max}$, the maximum one-sided translation is calculated as

$$x_{\max} = \frac{F_{x\max}}{K} = \frac{2\sigma_{\max}L^2}{3Eh} \tag{27}$$

where $\sigma_{\max}$ is the yield stress and E is Young's modulus of the material.

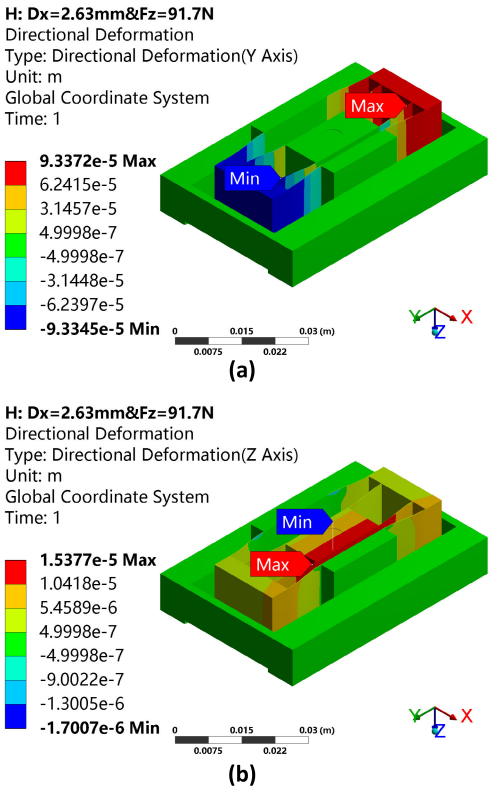

FIGURE 7. FEA results of the flexure joint: (a) y-axis deformation of the flexure joint; (b) z-axis deformation of the flexure joint.

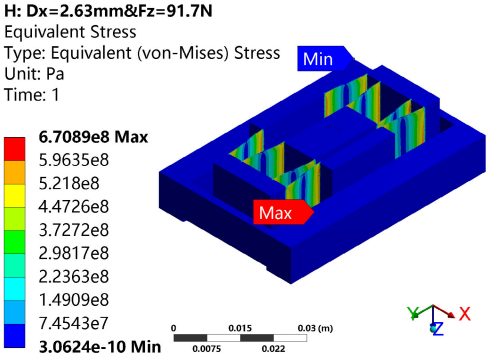

FIGURE 8. Stress distribution diagram of the flexure joint.

Eventually, Titanium alloy (Ti-5Al-2.5Sn) with $\sigma_{\max} = 8.27 \times 10^8\,\mathrm{N/m^2}$ and $E = 1.103 \times 10^{11}\,\mathrm{N/m^2}$ is selected for the double compound rectilinear flexure. With geometric parameters L=12 mm, h=0.2 mm and b=16 mm, the resulting stiffness in the drive direction is 16.34 N/mm, the stiffness ratio between z-axis and x-axis(the driving direction) is 1600:1. The maximum one-sided translation is 3.6 mm, which fulfills the translational displacement requirement of the three passive prismatic joints. As the payload is 275 N which is supported by three flexure joints, we conducted the finite element analysis(FEA) to verify the structure design of the flexure joints under the following conditions: 2.63 mm displacement in the x-axis direction and 91.7 N payload in the z-axis direction. As shown in Fig. 7, the deformations

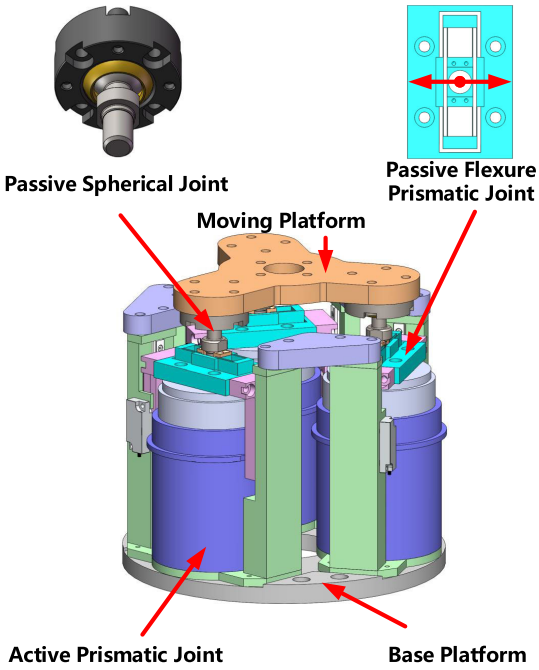

FIGURE 9. CAD model of the 3-DOF 2R1T end-effector.

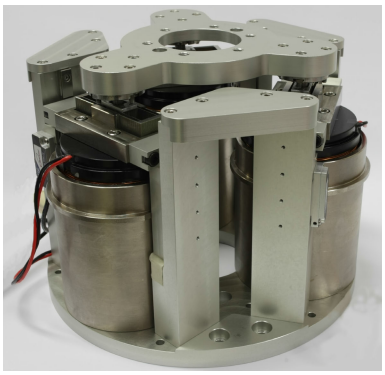

FIGURE 10. Prototype of the 3-DOF 2R1T end-effector.

of the moving platform in the y-axis and z-axis are within 0.5 μm and 15.4 μm, respectively, which verify that the double compound rectilinear flexure mechanism can significantly reduce the parasitic errors in off-axis directions. In Fig. 8, the FEA results indicate that the equivalent stress is 6.709×10^8 Pa, which is still within the yield stress of Titanium alloy. Moreover, the mass of a single flexure joint is about 90.3 g, which is far less than a conventional linear guide.

As a result, such a 3-PPS end-effector design with flexure-based passive prismatic joints can lead to lower moving mass, better dynamic performance and more compact structure. The CAD model of the 3-DOF 2R1T end-effector with flexure-based passive prismatic joints is designed, as shown in Fig. 9. A prototype of the 3-DOF 2R1T end-effector is fabricated, as shown in Fig. 10. The main structure as well as the moving platform is made of aluminum alloys to realize the light-weight design. Based on some primary

TABLE 1. The major technical specifications of the 3-DOF 2R1T end-effector prototype.

Technical specifications	Value
2R1T motion	$\pm 12^\circ \times \pm 12^\circ \times 25\,\text{mm}$
Mass	11 kg
Payload	275 N
Positioning accuracy	0.5 μm
Force control accuracy	0.5 N
Force control bandwidth	15 Hz

experimental verifications, the major technical specifications of the 2R1T end-effector prototype are obtained and listed in Table. 1.

VI. CONCLUSION

In this paper, kinematic design issues of a 3-DOF 2R1T end-effector with flexure joints for robotic finishing applications are addressed. The 3-PPS parallel mechanism is employed to achieve 3-DOF 2R1T ($\theta_x - \theta_y - Z$) motions, which is appropriate for curved surface polishing applications. As the 3-PPS parallel mechanism is featured with zero-torsion motion characteristic, the orientation of the proposed 2R1T end-effector's moving platform can be represented by a rotation about an axis parallel to the base platform plane. In light of the geometric representation of moving platform orientation, the interesting relationships about the entries of the rotation matrix, and the perpendicular arrangement of the two prismatic joints in each leg, closed-form linear solutions for both forward and inverse displacement analyses are readily derived. Accordingly, the subsequent analyses, i.e., passive prismatic joint displacement, parasitic motion, velocity, singularity, and workspace analyses are significantly simplified. Critical kinematic design parameters are determined based on the application requirements. Based on a numerical workspace analysis method, the proposed design can achieve a singularity-free $\pm 12^\circ \times \pm 12^\circ \times 25$ mm workspace. Furthermore, as the displacements of the passive prismatic joints are within 2.63 mm, flexure-based prismatic joints are designed to replace the conventional heavy linear guides, which significantly reduces the moving mass. To further improve force control performance, three base-mounted VCMs are employed as the active prismatic joints. Future work will focus on the dynamic modeling and force control algorithms for the 3-DOF 2R1T end-effector with flexure joints.

ACKNOWLEDGMENT

Part of the research and design work reported here was conducted while the first author was with the Singapore Institute of Manufacturing Technology (SIMTech). The design and construction of the prototype was under the excellent care of SIMTech colleagues, and SIMTech sponsored the construction of the prototype, which are duly acknowledged.

REFERENCES

[1] Y. Guilin, "Applied industrial robotics," *Bull. Chin. Acad. Sci.*, vol. 30, no. 6, pp. 785–792, 2015.
[2] Z. Ma, A.-N. Poo, M. H. Ang, Jr., G.-S. Hong, and H.-H. See, "Design and control of an end-effector for industrial finishing applications," *Robot. Comput.-Integr. Manuf.*, vol. 53, pp. 240–253, Oct. 2018.
[3] R. Zhu, G. Yang, Z. Fang, M. Yang, C. Y. Chen, and C. Zhang, "Kinematic design of a 3-DOF force-controlled end-effector with flexure joints for robotic finishing applications," in *Proc. IEEE/ASME Int. Conf. Adv. Intell. Mechatronics (AIM)*, Jul. 2019, pp. 1473–1478.
[4] Y. C. Sun and C. Y. Lai, *Handbook of Manufacturing Engineering and Technology*, vol. 4. London, U.K.: Springer, 2013, ch. 66, pp. 2445–2468.
[5] A. E. K. Mohammad, J. Hong, and D. Wang, "Design of a force-controlled end-effector with low-inertia effect for robotic polishing using macro-mini robot approach," *Robot. Comput.-Integr. Manuf.*, vol. 49, pp. 54–65, Feb. 2018.
[6] A. E. K. Mohammad, J. Hong, D. Wang, and Y. Guan, "Synergistic integrated design of an electrochemical mechanical polishing end-effector for robotic polishing applications," *Robot. Comput.-Integr. Manuf.*, vol. 55, pp. 65–75, Feb. 2019.
[7] L. Villani and J. De Schutter, *Springer Handbook of Robotics*, 2nd ed. Berlin, Germany: Springer-Verlag, 2016, ch. 9, pp. 195–220.
[8] E. A. Erlbacher, "Force control basics," *Ind. Robot, Int. J.*, vol. 27, no. 1, pp. 20–29, Feb. 2000.
[9] A. Sharon and D. Hardt, "Enhancement of robot accuracy using endpoint feedback and a macro-micro manipulator system," in *Proc. Amer. Control Conf.*, Jul. 1984, pp. 1836–1845.
[10] A. Sharon, N. Hogan, and D. E. Hardt, "The macro/micro manipulator: An improved architecture for robot control," *Robot. Comput.-Integr. Manuf.*, vol. 10, no. 3, pp. 209–222, Jun. 1993.
[11] O. Khatib, "Inertial properties in robotic manipulation: An object-level framework," *Int. J. Robot. Res.*, vol. 14, no. 1, pp. 19–36, Feb. 1995.
[12] U. Schneider, B. Olofsson, O. Sörnmo, M. Drust, A. Robertsson, M. Hägele, and R. Johansson, "Integrated approach to robotic machining with macro/micro-actuation," *Robot. Comput.-Integr. Manuf.*, vol. 30, no. 6, pp. 636–647, Dec. 2014.
[13] H. Zhang, H. Fang, Y. Fang, and B. Jiang, "Workspace analysis of a hybrid kinematic machine tool with high rotational applications," *Math. Problems Eng.*, vol. 2018, pp. 1–12, Jun. 2018.
[14] N. Mostashiri, J. S. Dhupia, A. W. Verl, and W. Xu, "A review of research aspects of redundantly actuated parallel robotsw for enabling further applications," *IEEE/ASME Trans. Mechatronics*, vol. 23, no. 3, pp. 1259–1269, Jun. 2018.
[15] T. Taunyazov, M. Rubagotti, and A. Shintemirov, "Constrained orientation control of a spherical parallel manipulator via online convex optimization," *IEEE/ASME Trans. Mechatronics*, vol. 23, no. 1, pp. 252–261, Feb. 2018.
[16] J. Wahl, "Articulated tool head," U.S. Patent 6 431 802, Aug. 13, 2002.
[17] D. Wang, L. Wang, J. Wu, and H. Ye, "An experimental study on the dynamics calibration of a 3-DOF parallel tool head," *IEEE/ASME Trans. Mechatronics*, vol. 24, no. 6, pp. 2931–2941, Dec. 2019.
[18] Y. Li and Q. Xu, "Kinematic analysis of a 3-PRS parallel manipulator," *Robot. Comput.-Integr. Manuf.*, vol. 23, no. 4, pp. 395–408, Aug. 2007.
[19] S. Liu, "Kinematic and dynamic analysis of a three-degree-of-freedom parallel manipulator," *J. Mech. Eng.*, vol. 45, no. 8, pp. 11–17, 2009.
[20] I. A. Bonev, "Direct kinematics of zero-torsion parallel mechanisms," in *Proc. IEEE Int. Conf. Robot. Autom.*, May 2008, pp. 3851–3856.
[21] Z. Huang, J. Wang, and Y. F. Fang, "Analysis of instantaneous motions of deficient-rank 3-RPS parallel manipulators," *Mech. Mach. Theory*, vol. 37, no. 2, pp. 229–240, Feb. 2002.
[22] J. Schadlbauer, D. R. Walter, and M. L. Husty, "The 3-RPS parallel manipulator from an algebraic viewpoint," *Mech. Mach. Theory*, vol. 75, pp. 161–176, May 2014.
[23] X.-J. Liu and J. Wang, *Parallel Kinematics: Type, Kinematics, and Optimal Design*. Berlin, Germany: Springer, 2014, ch. 3, pp. 81–119.
[24] G. Yang, T. J. Teo, I.-M. Chen, and W. Lin, "Analysis and design of a 3-DOF flexure-based zero-torsion parallel manipulator for nano-alignment applications," in *Proc. IEEE Int. Conf. Robot. Autom.*, May 2011, pp. 2751–2756.
[25] L.-W. Tsai, *Robot Analysis: The Mechanics of Serial and Parallel Manipulators*. Hoboken, NJ, USA: Wiley, 1999.
[26] J.-P. Merlet, *Parallel Robots*, vol. 128. Dordrecht, The Netherlands: Springer, 2006.
[27] G. Yang, W. Lin, S. Mustafa, I.-M. Chen, and S. Yeo, "Numerical orientation workspace analysis with different parameterization methods," in *Proc. IEEE Conf. Robot., Autom. Mechatronics*, Dec. 2006, pp. 1–6.
[28] Q. Xu, "Design and development of a compact flexure-based *XY* precision positioning system with centimeter range," *IEEE Trans. Ind. Electron.*, vol. 61, no. 2, pp. 893–903, Feb. 2014.

GUILIN YANG (Member, IEEE) received the B.E. and M.E. degrees from Jilin University, Changchun, Jilin, China, in 1985 and 1988, respectively, and the Ph.D. degree from Nanyang Technological University, in 1999, all in mechanical engineering.

From 1998 to 2013, he was a Senior Scientist with the Singapore Institute of Manufacturing Technology (SIMTech), Singapore, and the Manager of the Mechatronics Group. Since 2013, he has been with the Ningbo Institute of Materials Technology and Engineering, Chinese Academy of Sciences. He is currently a Professor, the Deputy President of the Ningbo Institute of Materials Technology and Engineering, and the Director of the Zhejiang Key Laboratory of Robotics and Intelligent Manufacturing Equipment Technology and Engineering. He has published over 270 technical articles in refereed journals and conference proceedings, authored three books, and filed 50 patents. His research interests include robotics and automation, such as precision electromagnetic actuators, compliant mechanisms, parallel-kinematics machines, cable-driven robots, modular robots, and robotic automation systems. He was a recipient of the R&D 100 Awards, in 2014.

RENFENG ZHU received the B.E. degree in process equipment and control engineering from the Taiyuan University of Technology, Taiyuan, Shanxi, China, in 2016. He is currently pursuing the Ph.D. degree in mechanical engineering with the University of Chinese Academy of Sciences, Beijing, China.

His research interests include analysis and design of force-controlled end-effectors, force control algorithm, and robotic system modeling.

ZAOJUN FANG received the B.E. degree from the University of Science and Technology, Anshan, Liaoning, China, in 2005, and the M.E. and Ph.D. degrees from the Institute of Automation, Chinese Academy of Sciences, Beijing, China, in 2008 and 2011, respectively.

He is currently a Professor with the Zhejiang Key Laboratory of Robotics and Intelligent Manufacturing Equipment Technology and Engineering, Ningbo Institute of Materials Technology and Engineering, Chinese Academy of Sciences, Ningbo, China. His current research interests include robot vision, robot control, and automation.

CHIN-YIN CHEN (Member, IEEE) received the B.S. and M.S. degrees from Dayeh University, Changhua, Taiwan, China, in 1998 and 2000, respectively, and the Ph.D. degree from National Sun Yat-sen University, Kaohsiung, Taiwan, in 2008.

He is currently a Professor with the Institute of Advanced Manufacturing Technology and the Ningbo Institute of Materials Technology and Engineering, Chinese Academy of Sciences, Ningbo, China. His research interests include actuators design, mechatronics, integrated structure/control design, and robotics. He was a Program Committee Member for more than the ten IEEE conferences.

CHI ZHANG (Senior Member, IEEE) received the B.E. and M.E. degrees from Xi'an Jiaotong University, Xi'an, Shanxi, China, in 1999 and 2002, respectively, and the Ph.D. degree from Nanyang Technological University, Singapore, in 2005.

He is currently a Professor and the Vice Director of the Zhejiang Key Laboratory of Robotics and Intelligent Manufacturing Equipment Technology and Engineering, Ningbo Institute of Materials Technology and Engineering, Chinese Academy of Sciences, Ningbo, China. He is also the Principle Investigator (PI) of the Precision Control and Advance Robotics Research Team. His current research interests include motor design and precision motion control.